Anodic and Cathodic Polarization of 1018 Mild Steel and 304 Stainless Steel

MSE 130: Experimental Materials Science and Design

Jonathan Lee
Department of Materials Science and Engineering
University of California, Berkeley

12 October 2020

Contents

1 Abstract

2 Introduction

The purpose of this report is to quantify the corrosion behavior of rod samples of 1018 mild carbon steel ("1018MS") and 304 stainless steel ("304SS") when polarized in strongly acidic solutions. In particular, the manufacturer has requested characterization in 1M HCl and 1M H_2SO_4, both of which have a pH of ~0, but which manifest different passivation behaviors at higher potentials due to their anion species.

2.1 Three Models for Polarization Curve Fitting

When a metal is placed in solution, there often exists a difference between the metal's work function and the electron energy levels of the solution species. Electrons will therefore transfer between the metal and the solution. Depending on the properties of the resulting metal ions, this may result in the corrosion (dissolution) of of the metal body. For example, for the coupled reactions in Equation 1, the Fe^{2+} ions produced are soluble in aqueous solution:

$$\begin{aligned} \mathrm{Fe}_{(s)} &\rightarrow \mathrm{Fe}^{2+}_{(aq)} + 2e^- \\ 2\mathrm{H}^+_{(aq)} + 2e^- &\rightarrow \mathrm{H}_{2(g)} \end{aligned} \tag{1}$$

In an isolated system, this redox reaction continues until a the unfavorable charge imbalance cancels the driving force; an equilibrium electrochemical potential difference is thus established. Yet the scenario is modified if this metal electrode is connected to a counter-electrode of a different metallic species. The counter-electrode may manifest its own redox reactions so as to maintain charge neutrality in the solution; furthermore, any electrochemical potential difference between the electrode and counter-electrode provides a driving force for current flow. The net effect is that a circuit is established that continuously corrodes the electrode.

This scenario is common in engineering situations – for example, the field of marine electronics deals heavily with the fact that the ocean-immersed components of a ship's hull will corrode if made of dissimilar metals. In the laboratory, it may be replicated within a polarization cell, wherein a sample is immersed in solution with a counter-electrode (typically Pt, which does not corrode) and a reference electrode against which to measure potential differences (such as the Saturated Calomel Electrode, a Hg-based electrode abbreviated as "SCE"). A potentiostat is used to drive the sample to various potentials relative to SCE; the current required to do so provides a measure of the reactions taking place at the sample surface. Such data sweeps are known as polarization curves.

The corrosion behavior of Fe in acidic solution may be described using the Butler-Volmer equation:

$$j = j_{\text{corr}} \left[\exp\left(\frac{\beta n F}{RT} (\phi - \Delta\phi_{\text{corr}}) \right) - \exp\left(\frac{(1-\beta) n F}{RT} (\phi - \Delta\phi_{\text{corr}}) \right) \right] \tag{2}$$

In this form of the Bulter-Volmer equation, ϕ is the applied potential relative to SHE. $\Delta\phi_{\text{corr}}$ is the "corrosion potential," at which the rates of Fe oxidation and H reduction at the electrode are equal to each other. The reaction rate at this point is the corrosion rate j_{corr} and manifests as a point where zero current need be supplied by the potentiostat. β encodes any anisotropy between the exchange current densities of the anodic and cathodic reactions and is typically ~0.5; $n = 2$ is the number of electrons exchanged in the reaction; R is the ideal gas constant; F is the Faraday constant; and T is temperature.

In this analysis, the Bulter-Volmer equation will not be used in its full form, but instead in three separate modified forms. The first modification is to condense and rewrite the prefactors:

$$j = j_{\text{corr}} \left[\exp\left(\frac{\ln(10)\eta}{A_{\text{Fe}}} \right) - \exp\left(\frac{\ln(10)\eta}{A_{\text{H}}} \right) \right] \tag{3}$$

In this case, η is shorthand for the overpotential $\phi - \Delta\phi_{\text{corr}}$. A_{Fe} and A_{H} are the Tafel slopes for Fe oxidation and H reduction, respectively, and may be considered as the overpotential required (in volts) to increase the reaction current density by a factor of 10. Fitting 3 to the polarization curve is typically done in the space of $\log_{10}|j|$ vs. η, such that either the anodic or cathodic terms dominate and produce linear behavior far from $\Delta\phi_{corr}$, while a singularity exists at $\Delta\phi_{corr}$ itself.

The second modification is to consider the Bulter-Volmer equation in the small-η regime, i.e. at potentials close to $\Delta\phi_{\mathrm{corr}}$ vs. SHE. A Taylor expansion of Equation 2 reveals linear behavior:

$$j = j_{\mathrm{corr}} \frac{nF}{RT} \eta \tag{4}$$

For the Fe/H corrosion couple, the nF/RT prefactor has a value of 77.85 V^{-1} at 25°C. The corrosion potential may therefore be determined by a linear fit to a "Linear Polarization Resistance" (LPR) scan at small overpotentials (colloqually defined as $|\eta| < 100$ mV).

The third modification is to account for the limitations of ion diffusion: at large overpotentials, a diffusion barrier may slow the rate of reaction, producing a smaller current than would be expected from Equation 2. Such diffusion barriers comprise complicated effects such as charge double-layers and may manifest themselves nonlinearly due to reaction kinetics, but as a rudimentary approximation, the barrier is assumed to have a constant resistivity ρ_{bar}. As such, a given half-reaction in Equation 2 will tend towards ohmic behavior at high currents, while Equation 2 itself describes electrical behavior comparable to a diode. The model in Reference [] for a diode and resistor in series may be used as a guide to derive:

$$j = \frac{1}{B_0 \rho_{\mathrm{bar}}} W(B_0 j_0 \rho_{\mathrm{bar}} \exp(B_0 \eta)) \tag{5}$$

In this equation, B_0 is defined as $ln(10)/A_0$ where A_0 is the Tafel-slope of the half-reaction, while W_0 is the 0-th branch of the Lambert W function. Since this equation is presented for a half-reaction, the parameters are defined in terms of a reference potential $\Delta\phi_{\mathrm{ref}}$ and reference current j_0 instead of a corrosion potential and current, which only have meaning for a reaction couple.

2.2 Additional Behavior: 1018MS

1018MS (0.15-0.20 wt% C, 0.60-0.90 wt% Mn, bal. Fe) possesses a heterogenous microstructure consisting of a nearly-carbonless ferrite α-phase and the high-carbon Fe_3C cementite phase. The fabrication of this steel involves quenching through a two-phase $\alpha + \gamma$ region; as a result, the original volumes of γ-phase become "pearlite," comprising dense lamellae of ferrite and cementite. An inspection of the Fe phase diagram for 0.18 wt% C indicates that 1018MS globally contains 2.7 wt% cementite, concentrated within pearlite regions that comprise 20 wt% of the microstructure. Cementite therefore comprises 14 wt% of the pearlite regions. For this analysis, the alloying element Mn is ignored.

This microstructure is generally expected to have a pronounced effect on the corrosion behavior of 1018MS. Cementite does not corrode as the high-Fe α-phase does, yet it comducts metallically and catalyzes the H^+ reduction reaction. Specifically, the exchange current density on Fe_3C for hydrogen reduction is several orders of magnitude higher than on the α-phase. As the α-phase corrodes away, Fe_3C lamellae are left behind, producing a large increase in the area available for Fe_3C to catalyze the reaction. This means that as the 1018MS electrode corrodes, the parameters of Equation 3 should shift towards greater corrosion currents in the cathodic regime.

2.3 Additional Behavior: 304SS

304SS (18 wt% Cr, 8 wt% Ni, bal. Fe) is designed to self-passivate in acidic solution above certain overpotentials. Specifically, at a passivation potential $\Delta\phi_{\text{pass}} > \Delta\phi_{\text{corr}}$, Cr atoms oxides into a +3 state in the form of a "passivation layer" consisting primarily of Cr_2O_3. Despite being only a few unit cells thick, this passivation layer provides an extremely-effective barrier against continued Fe oxidation; above the $\Delta\phi_{\text{pass}}$, the electrode current in a passivation sweep is nearly flat.

This passivated regime, however, has an upper limit resulting from a "breakdown potential" ($\Delta\phi_{\text{breakdown}}$) at which Cr_2O_3 begins to oxidize into aqueous $HCrO_4^-$ ions (+6 Cr oxidation state). In the presence of chloride ions, the limit is instead dictated by "pitting potential" ($\Delta\phi_{\text{pit}}$), wherein Cl^- ions locally attack the passivation barrier in a self-catalyzed reaction, thus locally restoring Fe corrosion behavior. This pitting potential typically occurs before the passivation layer breakdown potential; as such, the passivation regime in HCl is expected to be smaller than in H_2SO_4.

2.4 Charactization Targets

In light of the above discussion, the following quantities are desired in order to comprehensively characterize the samples from the manufacturer:

- 1018MS: $\Delta\phi_{\text{corr}}$, A_{Fe}, A_{H}, and effect of Fe_3C microstructural evolution.
- 304SS: $\Delta\phi_{\text{pass}}$, $\Delta\phi_{\text{breakdown}}$, $\Delta\phi_{\text{pit}}$, and any anomalous polarization behavior.

3 Experimental Procedure

1/8" diameter rods of 304SS and 1018MS were cut into cylindrical samples, then sanded with 600-grit paper and rinsed with deionized water so as to clean their surfaces. In total, four samples were produced (2x 304SS and 2x 1018MS). The samples were imaged under an optical microscope so as to provide a reference against which to compare their corroded surfaces.

Each sample was installed as the working electrode within a polarization cell, alongside a platinum counter-electrode and a saturated calomel reference electrode (SCE). So as to minimize the effects of solution resistivity on the measured voltage, the reference electrode was contained within a Lugger-Habin probe, of which the capillary tip was placed at the midpoint of the sample. The polarization cell was filled with either 250 mL of 1M HCl solution or 250 mL of 1M H2SO4 solution. The Luggin-Haber probe was filled with the same chosen solution to a surface level 1/4” below that of the polarization cell; this precluded the contamination of the polarization cell with 4M Cl- solution from the SCE reference. Care was taken during filling to avoid bubbles, as well as to position the Luggin-Haber probe in a way that would not allow bubbles to enter its capillary during the course of the experiment. Sample dimensions, solutions, and immersion lengths are recorded in Table 1.

Sample	Materials	Soln	Diameter	Immersed Length
1	1018MS	H_2SO_4	3.12 mm	14.8 mm
2	1018MS	HCl	3.12 mm	15.6 mm
3	304SS	H_2SO_4	3.12 mm	16.1 mm
4	304SS	HCl	3.12 mm	13.6 mm

Table 1: Sample dimensions used to calculate critical current densities from the collected current data.

The three electrodes were connected to a potentiostat constructed by previous laboratory personnel (10V compliance voltage, 190 mA maximum current, 200 mA thermal fuse cutoff, 15pA reference input current, 1e-6 mA current sensitivity, 2% current accuracy). The approximate location of the H/Fe corrosion potential was identified, after which various polarization sweeps were conducted for each sample. Twelve polarization sweeps were collected in total. The overall classification of each sweep are enumerated in Table 2, while the parameters governing each sweep are contained within the expanded Table 3 in Appendix 2. After the sweeps were concluded, the samples were dried and imaged once more under an optical microscope at magnifications of 5x, 10x, and 20x.

Scan	Sample	Solution	Classification	Sweep Rate (mV/sec)
1	1018MS	H2SO4	Ano/Cat	1 mV/sec
2	1018MS	H2SO4	LPR	0.1 mV/sec
3	1018MS	H2SO4	Ano/Cat	1 mV/sec
4	1018MS	H2SO4	LPR	0.1 mV/sec
5	1018MS	HCl	Ano/Cat	1 mV/sec
6	1018MS	HCl	LPR	0.1 mV/sec
7	1018MS	HCl	Ano/Cat	1 mV/sec
8	1018MS	HCl	LPR	0.1 mV/sec
9	304SS	H2SO4	Cathodic	1mV/sec
10	304SS	H2SO4	Anodic	1 mV/sec
11	304SS	HCl	Cathodic	1 mV/sec
12	304SS	HCl	Anodic	1 mV/sec

Table 2: General description of the 12 collected polarization curves. For the detailed parameters governing their collection, see Table 3 in Appendix 2.

Scan	Soln	Rate	Dir	A_H (V)	A_{Fe} (V)	j_{corr} (A/mm^2)	$\Delta\phi_{corr}$ (V)
0	H_2SO_4	1 mV/sec	Asc	8.778e-02	8.903e-02	1.784e-06	-4.794e-01
			Des	9.588e-02	8.833e-02	1.888e-06	-4.843e-01
2	H_2SO_4	10 mV/sec	Asc	8.341e-02	8.519e-02	1.663e-06	-4.730e-01
			Des	5.730e-02	8.076e-02	3.096e-06	-4.842e-01
4	HCl	1 mV/sec	Asc	7.706e-02	8.553e-02	1.277e-06	-5.022e-01
			Des	9.978e-02	8.326e-02	1.765e-06	-5.090e-01
6	HCl	10 mV/sec	Asc	7.490e-02	9.225e-02	1.469e-06	-4.806e-01
			Des	1.035e-01	8.415e-02	2.140e-06	-5.097e-01

Scan	Soln	Rate	Dir	$\sigma^2(A_H)$	$\sigma^2(A_{Fe})$	$\sigma^2(j_{corr})$	$\sigma^2(\Delta\phi_{corr})$	n
0	H_2SO_4	1 mV/sec	Asc	2.424e+02	2.786e+02	2.343e-15	1.401e-09	95
			Des	9.089e+00	1.206e+01	6.030e-15	3.785e-09	95
2	H_2SO_4	10 mV/sec	Asc	9.356e-06	1.890e-05	1.091e-13	3.618e-08	96
			Des	4.672e+00	8.336e+00	1.320e-14	7.072e-09	96
4	HCl	1 mV/sec	Asc	3.771e+01	4.110e+01	1.809e-15	3.614e-09	97
			Des	1.705e+03	1.066e+03	1.665e-15	7.201e-10	97
6	HCl	10 mV/sec	Asc	4.333e+02	2.297e+02	1.349e-15	1.066e-09	97
			Des	3.935e+03	8.564e+03	1.584e-15	2.366e-10	97

4 Results

4.1 1018MS Corrosion Parameters from Anodic/Cathodic Sweeps

4.2 1018MS Corrosion Parameters from LPR Sweeps

4.3 Deconvolution of 304SS Polarization Sweeps

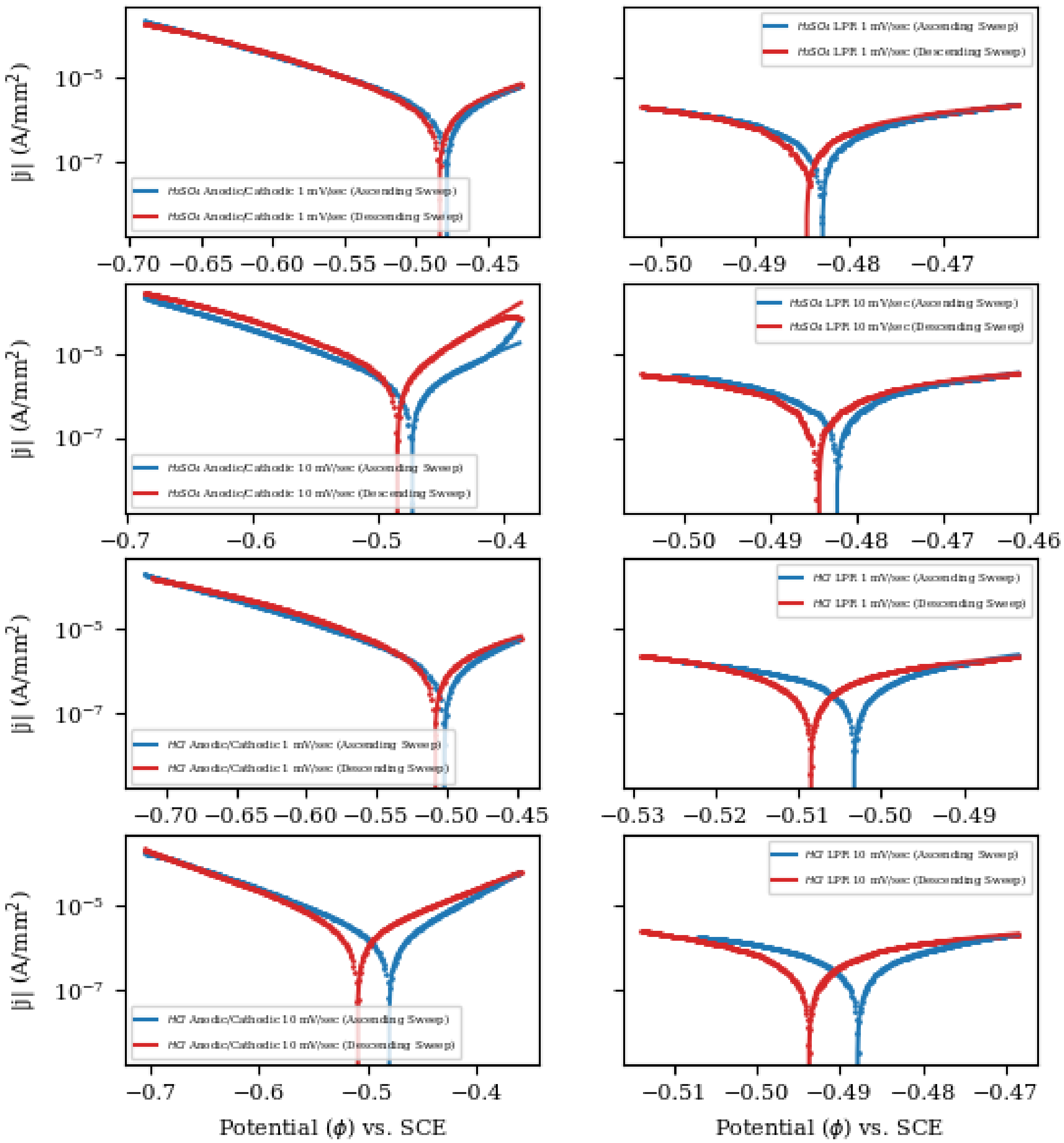

Scan	Sample	Solution	Classification	Sweep Rate (mV/sec)	Description

1	1018MS	H2SO4	Ano/Cat	1 mV/sec	Upward scan from 200 mV below CP to a potential above CP which produces 1 mA anodic current, followed by a reverse scan to return to the starting potential (200 mV below CP).
2	1018MS	H2SO4	LPR	0.1 mV/sec	After Scan 1, potential held at 200 mV until stable current, followed by an upward scan from 20 mV below CP to 20 mV above CP and a downward scan to return to 20 mV below CP.
3	1018MS	H2SO4	Ano/Cat	1 mV/sec	Upward scan from 200 mV below CP to a potential above CP which produces 10 mA anodic current, followed by a reverse scan to return to the starting potential (200 mV below CP).
4	1018MS	H2SO4	LPR	0.1 mV/sec	After Scan 3, potential held at 200 mV until stable current, followed by an upward scan from 20 mV below CP to 20 mV above CP and a downward scan to return to 20 mV below CP.
5	1018MS	HCl	Ano/Cat	1 mV/sec	Upward scan from 200 mV below CP to a potential above CP which produces 1 mA anodic current, followed by a reverse scan to return to the starting potential (200 mV below CP).
6	1018MS	HCl	LPR	0.1 mV/sec	After Scan 5, potential held at 200 mV until stable current, followed by an upward scan from 20 mV below CP to 20 mV above CP and a downward scan to return to 20 mV below CP.
7	1018MS	HCl	Ano/Cat	1 mV/sec	Upward scan from 200 mV below CP to a potential above CP which produces 10 mA anodic current, followed by a reverse scan to return to the starting potential (200 mV below CP).

8	1018MS	HCl	LPR	0.1 mV/sec	After Scan 7, potential held at 200 mV until stable current, followed by an upward scan from 20 mV below CP to 20 mV above CP and a downward scan to return to 20 mV below CP.
9	304SS	H2SO4	Cathodic	1 mV/sec	Downward scan from 20 mV above CP to 700 mV below CP.
10	304SS	H2SO4	Anodic	1 mV/sec	Upward scan from 20 mV below CP to the potential (1700 mV vs. SCE) that achieves maximum potentiostat current (190 mA), followed by a downward scan until the sample surface changes from anodic to cathodic (i.e. current sign flips).
11	304SS	HCl	Cathodic	1 mV/sec	Downward scan from 20 mV above CP to 700 mV below CP.
12	304SS	HCl	Anodic	1 mV/sec	Upward scan from 20 mV below CP to the potential (400 mV vs. SCE) that achieves maximum potentiostat current, followed by a downward scan until the sample surface changes from anodic to cathodic (i.e. current sign flips). Since the current in this sample/solution combination may continue to increase after switching scan direction, the direction was reversed in the vicinity of 100 mA instead of the maximum current (190 mA).

Table 3: Description of parameters for the 12 collected polarization curves.

10 Appendix 3: All Derived Parameters

11 Appendix 4: Surface Microscopy

Scan	Soln	Rate	Dir	j_{corr} (A/mm^2)	$\Delta\phi_{corr}$ (V)	$\sigma^2(j_{corr})$	n
1	H_2SO_4	1 mV/sec	Asc	1.342e-06	-4.830e-01	6.559e-16	338
			Des	1.354e-06	-4.841e-01	3.434e-15	421
3	H_2SO_4	10 mV/sec	Asc	2.058e-06	-4.822e-01	2.552e-15	342
			Des	1.941e-06	-4.849e-01	1.070e-14	444
5	HCl	1 mV/sec	Asc	1.302e-06	-5.032e-01	4.275e-14	353
			Des	1.335e-06	-5.085e-01	2.300e-14	442
7	HCl	10 mV/sec	Asc	1.265e-06	-4.879e-01	4.494e-15	342
			Des	1.297e-06	-4.937e-01	2.720e-14	443

Reaction	ϕ_0 (V)	j_0 (A/mm^2)	A (V)	ρ_{lim} (Ω·mm)
H^+ reduction	-3.728e-01	-9.612e-08	-1.138e-01	1.587e+02
Fe oxidation (passivation-limited)	-3.927e-01	7.891e-07	3.505e-03	3.905e+04
Cr_2O_3 barrier breakdown (asc)	9.688e-01	9.902e-07	3.701e-02	1.968e+03
H_2O breakdown (asc)	1.596e+00	1.065e-04	2.025e-01	3.230e-312
unknown reduction reaction	1.500e-01	-5.000e-11	-3.289e-02	2.000e+05
Cr_2O_3 solution deposition	1.070e+00	-1.812e+169	-9.784e-06	4.502e+06
Cr_2O_3 barrier breakdown (desc)	9.814e-01	4.565e-07	5.713e-02	1.324e+03
H_2O breakdown (desc)	1.599e+00	1.016e-04	1.971e-01	3.765e-06

Reaction	ϕ_{pass} (V)	α_{pass} (V^{-3})	ρ_{pass} (Ω·mm)
Fe oxidation (passivation-limited)	-3.530e-01	4.814e+00	6.966e+06
Cr_2O_3 barrier breakdown (asc)	1.300e+00	8.971e-03	5.670e+07
unknown reduction reaction	-3.000e-02	1.000e+01	1.000e+07
Cr_2O_3 barrier breakdown (desc)	1.239e+00	7.470e-03	2.868e+07

Reaction	ϕ_0 (V)	j_0 (A/mm^2)	A (V)	ρ_{lim} (Ω·mm)
H^+ reduction	-3.478e-01	-3.793e-07	-1.145e-01	3.210e+02
Fe oxidation (diffusion-limited)	-4.695e-01	1.498e-08	3.570e-02	2.157e+03
Fe oxidation (passivation-limited)	-4.695e-01	1.498e-08	3.570e-02	2.157e+03
Cl^- ion pitting	3.928e-01	8.802e-05	4.837e-02	9.837e+01

Reaction	ϕ_{pass} (V)	α_{pass} (V^{-3})	ρ_{pass} (Ω·mm)
Fe oxidation (passivation-limited)	-1.643e-01	5.187e+03	5.946e+03

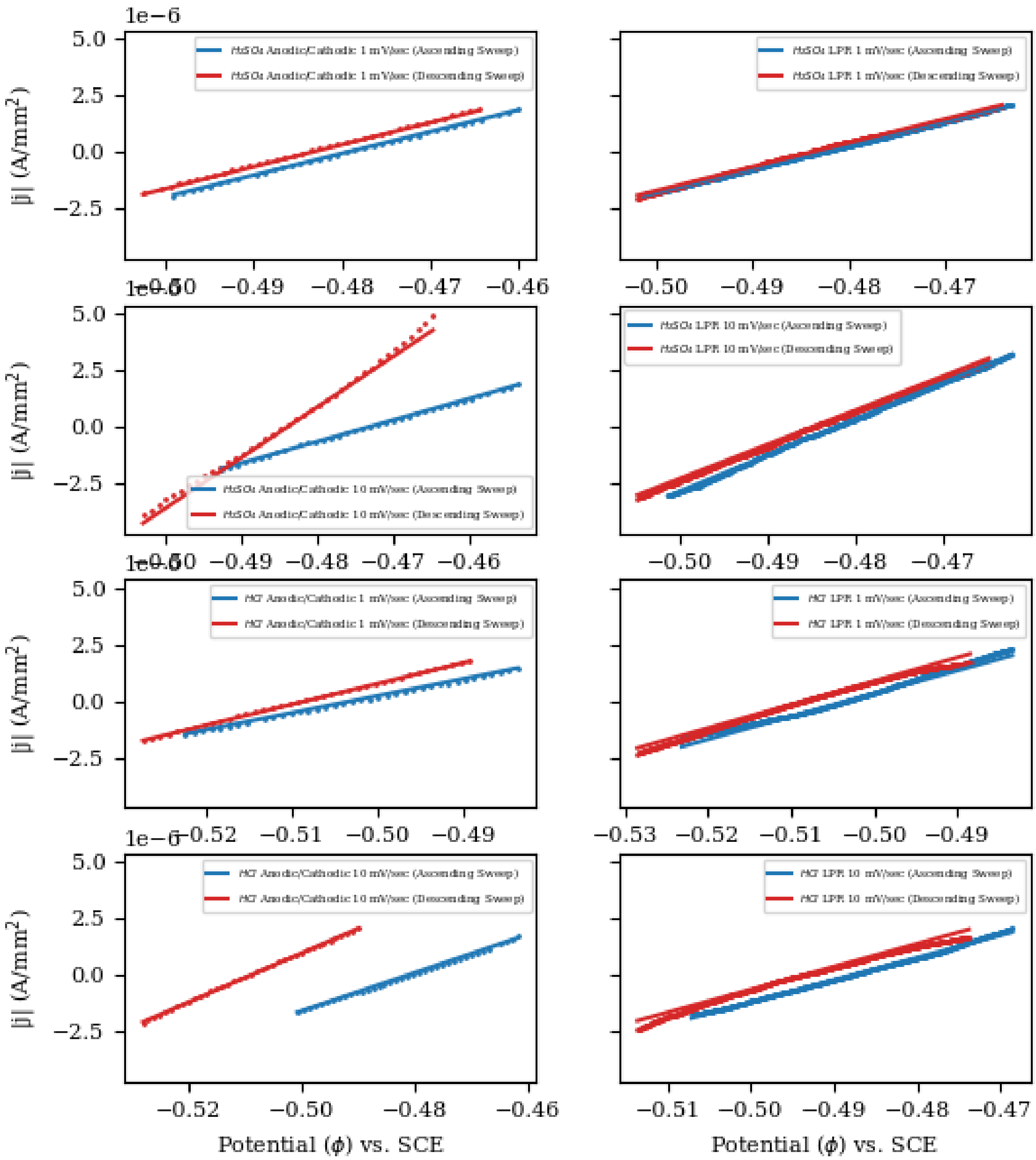
1e−6
|j| (A/mm^2)
H_2SO_4 Anodic/Cathodic 1 mV/sec (Ascending Sweep)
H_2SO_4 Anodic/Cathodic 1 mV/sec (Descending Sweep)
H_2SO_4 LPR 1 mV/sec (Ascending Sweep)
H_2SO_4 LPR 1 mV/sec (Descending Sweep)
H_2SO_4 Anodic/Cathodic 10 mV/sec (Ascending Sweep)
H_2SO_4 Anodic/Cathodic 10 mV/sec (Descending Sweep)
H_2SO_4 LPR 10 mV/sec (Ascending Sweep)
H_2SO_4 LPR 10 mV/sec (Descending Sweep)
HCl Anodic/Cathodic 1 mV/sec (Ascending Sweep)
HCl Anodic/Cathodic 1 mV/sec (Descending Sweep)
HCl LPR 1 mV/sec (Ascending Sweep)
HCl LPR 1 mV/sec (Descending Sweep)
HCl Anodic/Cathodic 10 mV/sec (Ascending Sweep)
HCl Anodic/Cathodic 10 mV/sec (Descending Sweep)
HCl LPR 10 mV/sec (Ascending Sweep)
HCl LPR 10 mV/sec (Descending Sweep)
Potential (ϕ) vs. SCE

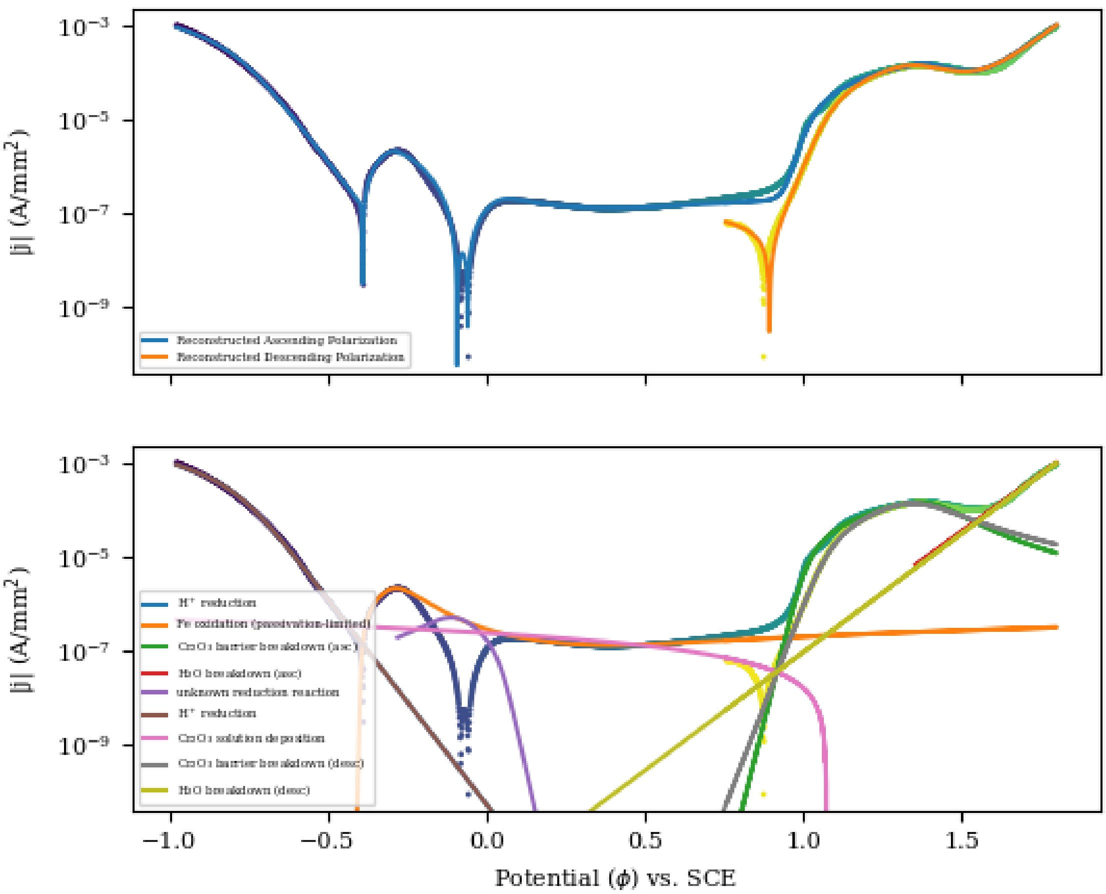

10^{-3}
10^{-5}
10^{-7}
10^{-9}
|j| (A/mm^2)
Reconstructed Ascending Polarization
Reconstructed Descending Polarization
H^+ reduction
Fe oxidation (passivation-limited)
Cr_2O_3 barrier breakdown (asc)
H_2O breakdown (asc)
unknown reduction reaction
H^+ reduction
Cr_2O_3 solution deposition
Cr_2O_3 barrier breakdown (desc)
H_2O breakdown (desc)
−1.0
−0.5
0.0
0.5
1.0
1.5
Potential (ϕ) vs. SCE

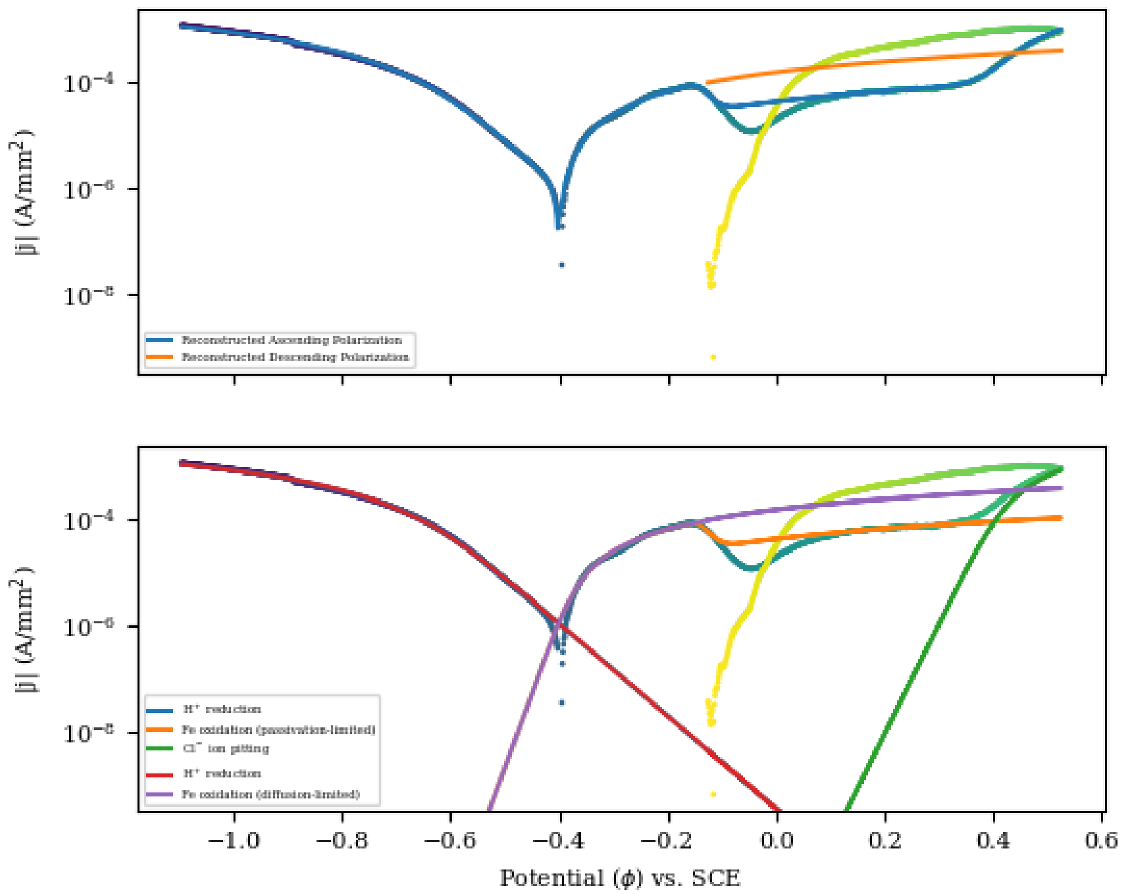

10^{-4}
10^{-6}
10^{-8}
$|j|$ (A/mm^2)
Reconstructed Ascending Polarization
Reconstructed Descending Polarization
10^{-4}
10^{-6}
10^{-8}
$|j|$ (A/mm^2)
H^+ reduction
Fe oxidation (passivation-limited)
Cl^- ion pitting
H^+ reduction
Fe oxidation (diffusion-limited)
−1.0
−0.8
−0.6
−0.4
−0.2
0.0
0.2
0.4
0.6
Potential (ϕ) vs. SCE